

Revisiting the paper “Using radiometric surface temperature for surface energy flux estimation in Mediterranean drylands from a two-source perspective”

William P. Kustas¹, Hector Nieto ², Laura Morillas³, Martha C. Anderson¹, Joseph G. Alfieri¹,
Lawrence E. Hipps⁴, Luis Villagarcía⁵, Francisco Domingo⁶, Monica Garcia^{7,8}

¹USDA-ARS Hydrology and Remote Sensing Lab, Beltsville, MD

²Spanish Research Council Institute for Sustainable Agriculture, Córdoba, Spain

³Department of Earth, Ocean and Atmospheric Sciences, University of British Columbia, Vancouver, Canada

⁴Department of Biometeorology and Climatology, Utah State University, Logan UT

⁵Department of Physical, Chemical and Natural Systems, Universidad Pablo de Olavide, ES-1013 Seville, Spain

⁶Estación Experimental de Zonas Áridas, Consejo Superior de Investigaciones Científicas (EEZA-CSIC), Almería, Spain

⁷Department of Environmental Engineering, Denmark Technical University (DTU), Kgs. Lyngby, Denmark.

⁸International Research Institute for Climate and Society (IRI). Columbia University, NY.

1 **Abstract:**

2

3 The recent paper by Morillas et al. [Morillas, L. et al. Using radiometric surface temperature for
4 surface energy flux estimation in Mediterranean drylands from a two-source perspective, Remote
5 Sens. Environ. 136, 234-246, 2013] evaluates the two-source model (TSM) of Norman et al.
6 (1995) with revisions by Kustas and Norman (1999) over a semiarid tussock grassland site in
7 southeastern Spain. The TSM - in its current incarnation, the two-source energy balance model
8 (TSEB) - was applied to this landscape using ground-based infrared radiometer sensors to
9 estimate both the composite surface radiometric temperature and component soil and canopy
10 temperatures. Morillas et al. (2013) found the TSEB model substantially underestimated the
11 sensible H (and overestimated the latent heat LE) fluxes. Using the same data set from Morillas
12 et al. (2013), we were able to confirm their results. We also found energy transport and
13 exchange behavior derived from primarily the observations themselves to differ significantly

14 from a number of prior studies using land surface temperature for estimating heat fluxes with
15 one-source modeling approaches in semi-arid landscapes. However, revisions to key vegetation
16 inputs to TSEB and the soil resistance formulation resulted in a significant reduction in the bias
17 and root mean square error (RMSE) between model output of H and LE and the measurements
18 compared to the prior results from Morillas et al (2013). These included more representative
19 ground-based vegetation greenness and local leaf area index values as well as modifications to
20 the coefficients of the soil resistance formulation to account for the very rough (rocky) soil
21 surface conditions with a clumped canopy. This indicates that both limitations in remote
22 estimates of biophysical indicators of the canopy at the site and the lack of adjustment in soil
23 resistance formulation to account for site specific characteristics, contributed to the earlier
24 findings of Morillas et al. (2013). This suggests further studies need to be conducted to reduce
25 the uncertainties in the vegetation and land surface temperature input data in order to more
26 accurately assess the effects of the transport exchange processes of this Mediterranean landscape
27 on TSEB formulations.

28 **Introduction**

29

30 Reporting errors in the modeled latent heat flux (LE) of approximately 90% mostly due to
31 a significant underestimate of the sensible heat flux (H) (70 Wm^{-2}), the recent study by Morillas
32 et al. (2013) suggests that the two-source energy balance (TSEB) model, which has been
33 successfully applied to a wide variety of landscapes and climates (Kustas and Anderson, 2009),
34 could not produce reliable estimates of LE in a semiarid Mediterranean tussock grassland site in
35 southeast Spain (Balsa Blanca). The Balsa Blanca site is representative of arid regions which
36 cover ~25 % of the Earth's land surface (Fensholt et al., 2012) and are characterized by having
37 low LE fluxes resulting in H being the dominant turbulent flux during most of the year (Ryu et
38 al. 2008). To better understand the factors adversely affecting the utility of the TSEB model in
39 this very heterogeneous semiarid environment, where the average daytime LE was about 115 W
40 m^{-2} , an analysis of the local flux-gradient relationship was conducted using a combination of the
41 measurements from the eddy covariance flux tower and the observed surface-air temperature
42 differences. In addition, based on other observations from the Balsa Blanca site suggesting
43 modification of TSEB resistance and canopy transpiration formulations from the standard, the
44 TSEB results are re-analyzed. Reaffirming an earlier study by Villagarcia et al. (2007) that
45 suggested that this landscape has some unique aerodynamic characteristics, the results of the
46 analysis presented here indicate that the flux-gradient behavior observed at the Balsa Blanca site
47 is quite different from what has been observed in prior studies over semiarid areas using surface-
48 air temperature differences to estimate surface fluxes (e.g., Stewart et al., 1994; Troufleau et al.,
49 1997; Verhoef et al., 1997). However, using local observations of vegetation cover conditions in
50 combination with revisions to some of the TSEB formulations, the unique flux-exchange

51 characteristics suggested by the observations can be accommodated by the model and the bias in
52 the H and LE greatly reduced.

53 In this investigation, the measurements from the Balsa Blanca flux tower are used to
54 compute the effective resistances to the transport of sensible heat, following the single-source
55 approach with radiometric surface temperature as the boundary condition (Stewart et al. 1994).
56 By examining values of the ratio of roughness lengths for momentum (z_{om}) and heat (z_{oh})
57 exchange with the single-source approach, which is indicative of the relative efficiency of
58 momentum versus heat transport, we found that the ratio of roughness lengths at this site departs
59 significantly from that at many other semi-arid sites analyzed by Stewart et al. (1994) among
60 others. This difference in momentum versus heat transport in many past studies is quantified in
61 terms of the variable kB^{-1} [$= \ln(z_{om}/z_{oh})$], which is discussed below, and its magnitude for the
62 Balsa Blanca is found to be similar to values derived theoretically and from observations for
63 fully vegetated surfaces (Brutsaert, 1982; Massman, 1999). Consequently, any current
64 thermally-based single-source technique using the measurements from Morillas et al. (2013)
65 would likely produce large errors in H and LE without *a priori* calibration of kB^{-1} .

66 It is important for the reader to understand that kB^{-1} originally accounted for the higher
67 efficiency of momentum versus heat transport from soil and vegetated surfaces, which comes
68 from the fact that very close to the surface elements heat transfer occurs by diffusion while
69 momentum transfer occurs by both viscous and pressure forces (Thom, 1972). With the use of
70 radiometric surface temperature in single-source approaches there is added complexity in
71 defining a kB^{-1} to account not only for key factors affecting aerodynamic transport of heat versus
72 momentum but also surface properties (notably fractional vegetation cover) and sensor viewing
73 angle affecting radiometric surface temperature observations (see discussion below).

74 We also find with TSEB that using ground-based local estimates of leaf area index (LAI)
75 and local green vegetation fraction (f_G), as opposed to using MODIS-derived estimates of local
76 LAI and f_G as in the Morillas study, there is a significant reduction in bias between TSEB model
77 and measured fluxes. In addition, adjustments to the empirical coefficients in the TSEB soil
78 resistance formulation based on visual inspection of the site indicating a rocky rough soil surface
79 further improved agreement between measured and modeled fluxes. This result indicates that
80 modifications to model inputs as well as some of the algorithms for modeling the turbulent
81 exchange are required in order to markedly improve model-measurement agreement at this semi-
82 arid flux site.

83 **Methodology**

84 As shown in Fig. 1a, single-source or bulk transfer schemes for modeling sensible heat
85 flux (H) often employ an additional resistance term (R_H) because heat transport is less efficient
86 than momentum transport from land surface (see e.g., Garratt and Hicks, 1973). However, in
87 applications of remotely sensed land surface temperature, an additional radiative resistance term
88 is added (represented by R_R) so that the total excess resistance (R_{EX}) is defined, namely $R_{EX} = R_H$
89 $+ R_R$ and accounts for the numerous factors that cause differences between the remotely-sensed
90 surface temperature and the aerodynamic surface temperature, most notably sensor view angle
91 and vegetation cover effects. The aerodynamic surface temperature is defined in Fig. 1 as either
92 T_{AEROH} or T_{AEROM} , which is physically coupled to the sensible heat exchange and associated
93 aerodynamic resistance R_{AERO} . If it is assumed there is no difference in the efficiency in heat and
94 momentum transport ($z_{oh} = z_{om}$ or $kB^{-1}=0$) then T_{AEROM} is associated with R_{AERO} while assuming
95 additional resistance to heat exchange results in computing T_{AEROH} from $R_{AH}(=R_{AERO} + R_H)$,
96 requiring $z_{oh} < z_{om}$ or $kB^{-1}>0$ (Kustas et al., 2007).

97 Due to the difficulty in parameterizing R_{EX} robustly and parsimoniously in the application
98 of the one-source scheme for different landscapes, climates, and observational configurations,
99 the two-source modeling approach was developed. Because it considers vegetation and soil
100 layers separately (Fig. 1b), this approach can accommodate the major factors that influence
101 differences between radiometric or remotely-sensed surface temperature and the aerodynamic
102 surface temperature which is explicitly defined in the two-source formulation (Kustas, 1990;
103 Norman et al., 1995). The different roles of soil and vegetation in the convective and radiometric
104 processes can be represented in a simplified form by a two-source model, such as TSEB, without
105 requiring any additional input information beyond that needed by single-source models using
106 more sophisticated kB^{-1} parameterizations (Norman et al., 1995; Kustas and Norman, 1999).

107 *Single-source formulation:*

108 According to Merlin and Chebhouni, (2004) one-source model formulations can provide
109 reliable fluxes, if the excess resistance term, R_{EX} , is calibrated for a given site. The problem is
110 that applying the R_{EX} formulation to another landscape often leads to poor results, indicating a
111 lack of generality to the relationships (e.g., Verhoef et al., 1997). On the other hand, there have
112 been several formulations derived from applying more complex soil-vegetation-atmosphere-
113 transfer (SVAT) models for estimating R_{EX} or kB^{-1} based on vegetation cover conditions and
114 radiometer viewing angle (Boulet et al., 2012; Lhomme et al., 2000; Matsushima, 2005) yielding
115 satisfactory results using a single-source approach. Such attempts to relate R_{EX} to vegetation and
116 surface properties are shown to mainly affect the value of R_R (Kustas et al., 2007). However,
117 regardless of whether or not R_{EX} values appropriate for a particular landscape can be estimated
118 from SVAT-derived formulations, computing R_{EX} from the remotely sensed surface temperature

119 and heat flux measurements does provide a metric quantifying the efficiency of heat exchange
 120 from the observations, themselves. In the context of the one-source model, H can be expressed
 121 as:

$$122 \quad H = \rho C_p \frac{T_{COMP} - T_A}{R_{AERO} + R_{EX}} \quad (1)$$

123 where ρC_p is the volumetric heat capacity of air, T_{COMP} is the “composite radiometric (remotely-
 124 sensed) land surface temperature”, T_A is the air temperature in the surface layer, and R_{AERO} is
 125 the aerodynamic resistance (Verma, 1989). Given measurements of T_{COMP} and T_A , H and
 126 estimates of R_{AERO} , which can have several forms as described by Verma (1989; see also e.g.,
 127 Stewart et. al., 1994; Verhoef et al., 1997), the value of the excess resistance term, R_{EX} , can be
 128 computed via Eq. (1). Two commonly used forms for estimating R_{AERO} , which differ in the
 129 stability correction functions applied to the logarithmic expressions, are:

$$130 \quad R_A = \frac{[\ln(\frac{z-d}{z_{om}}) - \psi_m][\ln(\frac{z-d}{z_{om}}) - \psi_h]}{uk^2} \quad (2a)$$

$$131 \quad R_{AM} = \frac{[\ln(\frac{z-d}{z_{om}}) - \psi_m][\ln(\frac{z-d}{z_{om}}) - \psi_m]}{uk^2} \quad (2b)$$

132 where z is the measurement height of mean wind speed, u , and air temperature, T_A , d is the
 133 displacement height, z_{om} is the aerodynamic roughness length (momentum roughness length), k is
 134 von Karman’s constant ($k = 0.4$), ψ_m is the surface layer stability correction function for wind,
 135 and ψ_h is the stability correction function for temperature. Since the friction velocity (u_*) is
 136 defined as $u_* = uk\{\ln[(z - d)/z_{om}] - \psi_m\}^{-1}$, R_{AM} can be computed directly from the
 137 measurements of u and u_* collected via a three-dimensional sonic anemometer according to

138 $R_{AM} = u/u_*^2$. To calculate R_A , the roughness parameters were estimated from canopy height (h_c)
 139 using well-established empirical relationships, namely $z_{om} = 0.13h_c$ and $d=0.6h_c$ (Brutsaert,
 140 1982), and the stability correction functions proposed by Brutsaert (1992).

141 As discussed by Stewart et al. (1994), among others, a single resistance (R_{AH}) formulation
 142 that relates to the aerodynamic surface temperature T_{AEROH} to the heat flux-temperature gradient
 143 relationship (see Fig. 1a) has often historically been defined as follows:

$$144 \quad R_{AH} = \frac{\ln\left(\frac{z-d}{z_{om}}\right) - \psi_h}{u_* k} + \frac{\ln\left(\frac{z_{om}}{z_{oh}}\right)}{u_* k} \quad (3)$$

145 which then gives the following one-source formulation for sensible heat flux exchange:

$$146 \quad H = \rho C_p \frac{T_{AEROH} - T_A}{R_{AH}} \quad (4)$$

147 where R_{AERO} is represented in Eq. (3) by the first RHS term and R_H is represented by the second
 148 RHS term ($R_{AH} = R_{AERO} + R_H$). The R_H term is often expressed as the inverse of the Stanton
 149 number, B^{-1} , which is defined as $B^{-1} = k^{-1} \ln(z_{om}/z_{oh})$ (Owen and Thompson, 1963), normalized by
 150 u_* . Further, the product, $kB^{-1} [= \ln(z_{om}/z_{oh})]$, characterizes the difference in the efficiency of heat
 151 and momentum transport. As mentioned above, others do not make a distinction between the
 152 roughness length for heat and momentum and only relate the sensible heat exchange to the
 153 aerodynamic resistance R_{AERO} , so that in Eq. (4) T_{AEROM} defines the aerodynamic surface
 154 temperature (see Fig. 1). However this often results in even greater discrepancies between
 155 aerodynamic surface temperature computed via Eq. (4) and radiometric (remotely-sensed)
 156 surface temperature (Kustas et al., 2007).

157 *Two-source formulation:*

158 Within the TSEB scheme, there is flexibility to evaluate alternative formulations for the
159 resistances from soil (R_S) and canopy (R_X) and sensitivities to uncertainties in resistance
160 coefficients (McNaughton and van den Hurk, 1995; Choudhury and Monteith, 1988; Kustas and
161 Norman, 1999; Cammalleri et al., 2010) as well as different methods to parameterize the canopy
162 transpiration in order to obtain a solution based on the partitioning of radiometric temperature
163 and energy balance between soil and canopy elements (e.g., Colaizzi et al., 2014). Using the
164 standard TSEB parameterizations for R_S and R_X , we have the following

$$165 \quad R_S = \frac{1}{c(T_{SOIL} - T_{CANOPY})^{1/3} + bu_S} \quad (5)$$

166

167 and

$$168 \quad R_X = \frac{c'}{LAI} \sqrt{\left(\frac{l_W}{u_{d+z_{OM}}}\right)} \quad (6)$$

169

170 In the formulation for R_S , u_S is wind speed near soil surface (~ 0.05 m), T_{SOIL} and T_{CANOPY} are
171 radiometric temperatures and default values are $c = 0.0024$ ($\text{m s}^{-1} \text{K}^{-1/3}$) and $b = 0.012$ for
172 moderately rough soil surfaces (Kustas and Norman 1999). However, values up to $c \sim 0.0038$ m
173 $\text{s}^{-1} \text{K}^{-1/3}$ and b ranging from 0.034 to 0.087 are proposed in the literature (Kondo and Ishida 1997;
174 Sauer et al. 1995) for rough soil and partially vegetated surfaces. This is the case in the Balsa
175 Blanca, where there is considerable rock content on the soil surface and strongly clumped

176 vegetation. For R_X , l_W is the leaf size/width, and u_{d+zom} the wind speed at the level of effective
 177 momentum absorption by the canopy. A value for $C'=130 \text{ s}^{1/2} \text{ m}^{-1}$ was suggested by
 178 McNaughton and van den Hurk (1995), in comparison with the $90 \text{ s}^{1/2} \text{ m}^{-1}$ adopted by Norman et
 179 al. (1995). In the original version of the TSEB, an initial solution for the canopy transpiration
 180 component, LE_C , is obtained using the Priestley-Taylor formulation,

$$181 \quad LE_C = \alpha_{PTC} f_G \frac{\Delta}{\Delta + \gamma} R_{NC} \quad (7)$$

182 where $\alpha_{PTC} \sim 1.3$, Δ is the slope of the temperature-saturation vapor pressure curve, γ is
 183 the psychrometric constant, R_{NC} is the canopy net radiation, and f_G is the green vegetation
 184 fraction. Recent ground-based observations from the Balsa Blanca site indicate f_G was
 185 significantly lower than what was derived from the MODIS data and used in the Morillas study.

186 **Results with One-Source Model: Evaluating kB^{-1} Parameter**

187 In most studies evaluating one-source modeling approaches, no distinction is made
 188 between R_{EX} and R_H and the value of kB^{-1} is parameterized so that T_{COMP} and T_{AEROH} agree.
 189 Studies by Stewart et al. (1994), Verhoef et al. (1997), and Troufleau et al. (1997) evaluated kB^{-1}
 190 using Eq. (1) with R_{EX} approximated as $kB^{-1}/(u_* k)$ (based on $R_{EX} \approx R_H$ assumption) for several
 191 semiarid and arid sites. Since R_{AERO} computed using R_A and R_{AM} yielded similar results for the
 192 Balsa Blanca field site, the former was used in Eq. (1) to estimate kB^{-1} at this site for consistency
 193 with these previous studies.

194 Compared to the values of kB^{-1} from these earlier studies, the data from Balsa Blanca site
 195 yield values that are atypically low (Table 1). The values of kB^{-1} at the Balsa Blanca site, which
 196 averaged near 2, are more typical of those observed when the heat exchange occurs primarily

197 with permeable vegetative roughness elements (Brutsaert, 1982, Fig. 4.24) that make up fully-
198 vegetated surfaces (Garratt and Hicks, 1973). Based on both field observations (e.g., Kustas,
199 1990; Stewart et al., 1994) and modeling studies using a two-source model based on Lagrangian
200 theory (McNaughton and van den Hurk; 1995), the value of kB^{-1} can be as much as a factor of
201 ten larger when the soil surface also contributes significantly to heat exchange. The increase in
202 the value of kB^{-1} is due to the lower relative efficiency of heat exchange from the soil compared
203 to the exchange from the canopy elements that results from the greatly diminished winds near the
204 soil surface. Stated differently, larger kB^{-1} values reflect a reduction in the overall coupling
205 between the surface and the atmosphere, a behavior which is typically observed in semi-arid
206 sparsely vegetated landscapes. However, with a $kB^{-1} \sim 2$ this does not appear to be the case for
207 the Balsa Blanca site. Apart from the fractional cover and structural characteristics of the
208 vegetation, kB^{-1} values are also strongly affected by plant stress levels and micrometeorological
209 conditions causing kB^{-1} to change by a factor of 10 during the course of a day at the same site
210 (Lhomme et al., 1997). The uniqueness of this dataset is further demonstrated in Figure 2,
211 showing a histogram of kB^{-1} values derived from the Balsa Blanca data along with the mean and
212 standard deviations of the kB^{-1} values for all the sites listed in Table 1. A Z-test at the 95%
213 confidence level indicates the mean kB^{-1} value from Balsa Blanca data does not come from the
214 population of samples that generated the mean kB^{-1} values from the other sites in Table 1. In
215 other words, the mean $kB^{-1}=2.2$ falls outside the likely range of mean values observed at the
216 other semi-arid and arid sites.

217 The data set can also be visualized in terms of the implied ratio of the roughness lengths
218 for heat and momentum, z_{oh}/z_{om} . As can be seen in Figure 3, this ratio from the Balsa Blanca site
219 is an order of magnitude larger than the ratio observed for nearly all of the other sites. This

220 suggests the relative efficiency of heat exchange is much greater than has been typically
221 observed for sparsely-vegetated arid sites, if the radiometric temperature observations are indeed
222 representative of the entire site composite surface.

223 The “aerodynamic surface temperature”, T_{AEROH} , can be computed by inverting Eq. (4)
224 and using an *a priori* formulation for R_H (i.e., $R_H = kB^{-1}/u_* k$) according to:

$$225 \quad T_{AEROH} = T_A + \frac{HR_{AH}}{\rho C_p} \quad (8)$$

226 Using the observed values of H , T_A and u_* along with estimates of R_{AERO} using Eq. (2a), and
227 assuming kB^{-1} has a value of either 2, indicative of vegetated surfaces (Brutsaert, 1982), or 7, an
228 average from the semi-arid sites analyzed in Stewart et al. (1994), T_{AEROH} was calculated via Eq.
229 (8). As one would expect with kB^{-1} equaling ~ 2 , the derived T_{AEROH} is approximately equal to
230 T_{COMP} since for the Balsa Blanca site the average value of kB^{-1} equals 2.2, with T_{AEROH} values
231 falling slightly above and below the 1:1 line (Fig. 4a). However, when kB^{-1} is set equal to 7,
232 T_{AEROH} is significantly greater than T_{COMP} (Fig. 4b). This would suggest an unusual case where
233 the effective emitting surface temperature is *hotter* than the observed surface temperature during
234 the daytime hours.

235 At the Balsa Blanca site, having perennial grasses, the vegetation fractional cover remains
236 fairly constant, $f_c \sim 0.6$ (Morillas et al., 2013), hence midday soil - canopy temperature
237 differences ($T_{SOIL} - T_{CANOPY}$), by assuming $T_{COMP} = [f_c T_{CANOPY}^4 + (1 - f_c) T_{SOIL}^4]^{\frac{1}{4}}$, ranged from
238 2 °C to 12 °C over the growing season. This range in temperature difference between T_{SOIL} and
239 T_{CANOPY} is relatively small compared to soil - canopy temperature differences typically observed
240 in semi-arid environments, often exceeding 20 °C (e.g., Chebhouni et al., 2001; Humes et al.,

241 1994; Kustas et al., 2004). This is likely due in large part to the fact that plant green-up
242 coincides with the wet season in many semi-arid environments whereas in Mediterranean
243 ecosystems, the rainy period tends to be over the winter months while green-up of the vegetation
244 happens during the dry season. This leads to the vegetation generally having higher stress
245 conditions resulting in relatively higher values of T_{CANOPY} (Were et al., 2007; Verhoef et al.,
246 1996).

247 Applying Lhomme et al. (2000) expression for estimating B^{-1} with LAI adjusted for clumped
248 vegetation yields a kB^{-1} value of ~ 3.7 which results in a z_{oh}/z_{om} ratio of $\sim 1/40$ whereas kB^{-1} from
249 the observations yields a z_{oh}/z_{om} ratio of $\sim 1/9$. This again points to other measurement factors
250 and/or landscape features at Balsa Blanca that is affecting the efficiency of heat transport from
251 its surface. In a recent single-source model application using remotely sensed surface
252 temperature, modification to the soil resistance or the kB^{-1} expression for bare soil heat transfer
253 was required to improve heat flux predictions in the semi-arid Tibetan Plateau region (Chen et
254 al., 2013). Indeed, the single-source expression for heat transfer over bare soil surfaces derived
255 theoretically by Brutsaert (1975) shows a strong dependency of kB^{-1} on roughness Reynolds
256 number, and has been validated using remotely sensed surface temperature and sensible heat flux
257 observations (Cahill et al., 1997; Yang et. al., 2008).

258 **Results from TSEB --Before and After Modifications of Inputs: LAI and f_G and R_s**

259 Morillas et al. (2013) used the effective values of LAI from MODIS LAI/fAPAR
260 (fAPAR: fraction of absorbed photosynthetically active radiation) estimates (average between
261 the Terra MOD15A and Aqua MYD15A products), with a $f_C = 0.6$ from site measurements. The

262 value of f_G was estimated based on the empirical approach of Fischer et al (2008), with fAPAR
263 defined as well from MODIS LAI/fAPAR data.

264 Using recent observations made in the Balsa Blanca study site from a different year but
265 similar weather conditions, estimates of local green LAI were derived from monthly NDVI data
266 measured using a multi-spectral camera and field LAI sampling at the study site. The one-sided
267 leaf area index (LAI) was estimated for *Stipa tenacissima* from reflectance measurements with a
268 Tetracam ADC camera (Tetracam, Inc., Gainesville, FL, USA¹). This camera records images
269 with 2048×1536 pixels using an 8 mm lens and 8 mm focal length. The pictures were taken at a
270 height of 2 m to cover all the surface of the plants in one or two images. The plant canopy
271 reflectance was divided in red, green and NIR band of wavelengths by the optical filters of the
272 camera. The images were processed with the specific software delivered with the camera
273 (PixelWrench II) that allows adjust the factory calibration to the spectral balance of the ambient
274 light selecting in the picture a training area (a White Teflon Calibration Plate located near each
275 plant, also provided with the camera) and calculate NDVI or other vegetation indices. After this
276 correction, the pictures with the NDVI index were exported to the ESRI ArcMap software in
277 TIFF format to select only the pixels that represented the plant canopy, thereby eliminating the
278 noise caused by the surrounding soil. In our study, LAI values were calculated from an NDVI-
279 LAI relationship obtained by correlating NDVI values from the Tetracam ADC camera with LAI
280 values from destructive sampling.

281 Assuming total (green+dead) LAI is a constant value of ~1.75 over the growing season
282 (study period), which appears reasonable based on visual observations of the site (Fig. 5c), we
283 derived new values of f_G (Fig. 6) based on Tetracam ADC camera derived green LAI (Fig. 6b).

¹ The mention of trade names of commercial products in this article is solely for the purpose of providing specific information and does not imply recommendation or endorsement by the US Department of Agriculture.

284 Here, f_G was allowed to vary from 0, if the green LAI reached 0, up to 0.7 when green LAI
285 reached its maximum value, considering that there are always dead/senescent material in the
286 tussock grass over all seasons (Fig. 5b and 5c). The results of changing the LAI and f_G inputs in
287 TSEB from those used originally in the TSEB model run by Morillas et al. (2013) are illustrated
288 in Figure 7. There is a considerable reduction in the bias and RMSE for H and LE estimates
289 using the new LAI and f_G inputs in TSEB, which highlights the limitations of using MODIS
290 derived values of LAI and f_G at this site and the need of ground-based biophysical measurements
291 at the same spatial resolution as the radiometric surface temperature measurements for evaluating
292 TSEB model performance under such conditions.

293 Modifications to the empirical parameters c and b used to estimate soil resistance, R_s ,
294 were also made to better capture a more efficient heat exchange due to the rough soil surface and
295 greater intensity in the turbulence based on the significant rock content of the soil surface and
296 clumpiness of the vegetation (see Fig. 5). The values used in Eq.5 were $c = 0.0038$ (Kondo and
297 Ishida, 1997) and $b=0.065$ (average of the range in value reported by Sauer et al., 1995 for small
298 and developing canopies). This modification in R_s resulted in a further significant reduction in H
299 and LE bias, with TSEB estimates much closer to the 1:1 line, and considerably lower RMSE for
300 both fluxes (Fig. 7e and f). However for LE it resulted in a lower R^2 as a result of an increase in
301 scatter in H estimates. Using a larger resistance to heat exchange from the canopy with $C'=130$
302 instead of 90 in Eq. (6) as proposed by McNaughton and van den Hurk (1995) had little effect on
303 TSEB output of H and LE (results not shown). The implication of these results is that while the
304 bulk heat transport expressed in terms of the kB^{-1} parameter at the Balsa Blanca differs
305 significantly from earlier findings over most other semi-arid and arid surfaces using one-source
306 modeling approaches, the TSEB indicates that there are physical factors related to soil and

307 vegetation properties that largely contribute to this result. By using local observations of LAI
308 and f_G as inputs to TSEB and changing the soil resistance coefficients to be more representative
309 of the surface characteristics, the TSEB model achieves good agreement with H and LE
310 measurements.

311 **Conclusions**

312 While there can be limitations in applying TSEB in complex heterogeneous water-limited
313 environments having natural vegetation without modifications to the canopy transpiration
314 formulations (Agam et al., 2010; Guzinski et al., 2013; Chirouze et al., 2014), caution needs to
315 be exercised interpreting and using measurements made over such surfaces. In the case of the
316 Morillas et al. (2013) paper, the relationship of the radiometric surface temperature-air
317 temperature differences and heat flux exchange differ significantly from other semiarid areas
318 with partial vegetation cover as defined by the kB^{-1} variable used in single-source modeling
319 approaches.

320 For example, applying a mean value of $kB^{-1} = 7$, typical for semi-arid sparsely vegetated
321 surfaces derived by Stewart et al (1994), Stewart (1995) showed significant improvement in heat
322 flux estimation using T_{COMP} for a sparsely vegetated grassland site with LAI ~ 0.5 and fractional
323 vegetation cover $\sim 75\%$ in the in the Konza Prairie, Kansas, USA. However, the Konza Prairie
324 site is not strongly clumped as the Mediterranean tussock grassland in the Balsa Blanca nor has
325 as dry a climate.

326 Obviously, this same value for kB^{-1} would not be appropriate for the Balsa Blanca and is
327 indicative of the fact that while one-source modeling approaches using radiometric surface
328 temperature can provide a diagnostic tool for evaluating the efficiency of heat exchange, they are

329 not reliable in general for heat flux estimation without *a priori* calibration, particularly for
330 heterogeneous sites. However, their utility for heat flux estimation has improved through the
331 development of kB^{-1} formulations that account for fractional vegetation cover or LAI (Su et al.,
332 2001; Lhomme et al., 2000; Boulet et al., 2012) and variation in kB^{-1} for bare soil heat transport
333 (e.g., Chen et al., 2013).

334 The current findings require flux-gradient parameterization that is not typically observed
335 in any other previously studied semi-arid and arid sites, and with modifications to the TSEB soil
336 resistance parameters for a very rough soil surface and more efficient heat exchange as well as
337 modifications to the LAI and estimate of f_G based on ground observations, the significant
338 underestimate of H and overestimate of LE is greatly reduced. These revisions to both soil
339 resistance parameterizations and input data emphasize the need for detailed local measurements
340 to better understand model limitations and/or refinements necessary for different land cover
341 types.

342 While regional to global scale application of TSEB land surface scheme using a modeling
343 system based on coarse resolution satellite data called the Atmosphere Land Exchange Inverse
344 (ALEXI) model, which also has a Disaggregation scheme (DisALEXI) when using higher
345 resolution imagery (Anderson et al., 2011) is currently producing continental scale flux fields,
346 studies like the current one suggest this model is not applicable with a single set of resistance
347 parameterizations for all landscapes. On the other hand, results of such local studies can be
348 entered into a land use data base at satellite resolutions to refine model parameterizations for
349 certain regions found to be especially challenging.

350 This study also cautions on the use of local observations (radiometric surface
351 temperature) with non-local or larger scale estimates of other key inputs which are not
352 necessarily representative of local conditions (i.e., leaf area index, green fraction). Clearly,
353 additional measurements and analyses for this landscape are needed to confirm that these
354 modifications to TSEB resistances are warranted, which in addition should include more ground-
355 based infrared radiometer measurements as well as simultaneous local observations of LAI and
356 f_G . At the same time, application with satellite data for all model inputs should also be
357 performed to evaluate the limitations of remote sensing algorithms used in defining key model
358 inputs (e.g., Guzinski et al., 2013).

359 Finally, other two-source resistance formulations from Choudhury and Monteith (1988)
360 and McNaughton and van den Hurk (1995) should be evaluated to see if there is a consistency in
361 results using different two-source resistance formulations, which may help better understand the
362 observations and findings of Morillas et al. (2013).

363 **Acknowledgements:**

364 We would like to thank Dr. Laura Morillas, Professor Monica Garcia, Dr. Luis Villagarcía and
365 Dr. Francisco Domingo funded by Andalusia Regional Government projects (P06-RNM-01732,
366 P08-RNM-3721), European Union (ERDF funds) with support from the Spanish Ministry of
367 Science and Innovation (CGL2011-27493), the Danish Council for Independent Research and
368 Technology and Production Sciences (Grant 09-070382), for sharing the data used in the
369 Morillas et al. (2013) paper and for their contributions to the analysis in this paper. USDA is an
370 equal opportunity provider and employer.

371 **References:**

- 372 Anderson, M.C., Kustas, W.P., Norman, J.M., Hain, C.R., Mecikalski, J.R., Schultz, L.,
373 González-Dugo, M.P., Cammalleri, C., d’Urso, G., Pimstein, A., and Gao, F. 2011. Mapping
374 daily evapotranspiration at field to continental scales using geostationary and polar orbiting
375 satellite imagery, *Hydrol. Earth Syst. Sci.* 15, 223-239, DOI: 10.5194/hess-15-223-2011.
376
- 377 Agam, N., Kustas, W.P., Anderson, M.C., Norman, J.M., Colaizzi, P.D., Howell, T.A., Prueger,
378 J.H., Meyers, T.P., Wilson, T.B. 2010. Application of the Priestley-Taylor Approach in a Two-
379 Source Surface Energy Balance Model. *J. Hydrometeorol.*, 11 (1):185-198.
- 380 Boulet, G., Olioso, A., Ceschia, E., Marloie, O., Coudert, B., Rivalland, V., Chirouze, J.,
381 Chehbouni, G. 2012. An empirical expression to relate aerodynamic and surface temperatures for
382 use within single-source energy balance models. *Agric.Forest Meteorol.*, 161: 148-155.
- 383 Brutsaert, W. 1975. A theory for local evaporation (or heat transfer) from rough and smooth
384 surfaces at ground level. *Water Resour. Res.*, 11:543-550.
- 385 Brutsaert, W. 1982. *Evaporation into the atmosphere*. D. Reidel Pub. Co., Dordrecht, Holland, 299
386 pp.
- 387 Brutsaert, W. 1992. Stability correction functions for the mean wind speed and temperature in
388 the unstable surface layer. *Geophys. Res. Lett.*, 19, 469-472.
- 389 Cahill, A.T., Parlange, M.B., and Albertson, J.D. 1997. On the Brutsaert temperature roughness
390 length model for sensible heat flux estimation. *Water Resour. Res.*, 33(10):2315-2324.
- 391 Cammalleri, C., Anderson, M.C., Giraolo, G., d’Urso, G., Kustas, W.P., La Loggia, G.,
392 Minacapilli, M. 2010. The impact of in-canopy wind profile formulations on heat flux estimation

393 in an open orchard using the remote sensing-based two-source model. *Hydrol Earth Syst. Sci.*
394 14:2643-2659.

395

396 Chehbouni A., Nouvellon, Y., Lhomme, J-P., Watts, C., Boulet, G., Kerr, Y. H., Moran, M. S.,
397 Goodrich, D. C. 2001. Estimation of surface sensible heat flux using dual angle observations of
398 radiative surface temperature. *Agric. For. Meteorol.* 108:55-65.

399

400 Chen, X.L., Su, Z.B., Ma, Y.M., Yang, K., Wen, J., Zhang, Y. 2013. An Improvement of
401 Roughness Height Parameterization of the Surface Energy Balance System (SEBS) over the
402 Tibetan Plateau. *J. Appl. Meteorol. Climatol.*, 52(3): 607-622.

403

404 Chirouze, J., Boulet, G., Jarlan, L., Fieuzal, R., Rodriguez, J.C., Ezzahar, J., Er-Raki, S.,
405 Bigeard, G., Merlin, O., Garatuza-Payan, J., Watts, C., Chebhouni, G. 2014. Intercomparison of
406 four remote-sensing –based energy balance models to retrieve surface evapotranspiration and
407 water stress of irrigated fields in semi-arid climate. *Hydrol. Earth Syst. Sci.* 18:1165-1188

408

409 Choudhury, B.J., Monteith, J.L., 1988. A four-layer model for the heat budget of homogeneous
410 land surfaces. *Quart. J. R. Meteorol. Soc.* 114 (480), 373 – 398.

411

412 Colaizzi, P.D., Agam, N., Tolk, J.A., Evett, S.R., Howell, T.A., Gowda, P., O’Shaughnessy,
413 S.A., Kustas, W.P., Anderson, M.C. 2014. Two-source energy balance model to calculate E, T,
414 and ET: Comparison of Priestley – Taylor and Penman – Monteith formulations and two time
415 scaling methods. *Tran. ASABE.* 57(2):479-498.

416

417 Fensholt, R., Langanke, T., Rasmussen, K., Reenberg, A., Prince, S.D., Tucker, C., Scholes, R.J.,
418 Le, Q.B., Bondeau, A., Eastman, R., Epstein, H., Gaughan, A.E., Hellden, U., Mbow, C., Olsson,
419 L., Paruelo, J., Schweitzer, C., Seaquist, J., and Wessels, K. 2012. Greenness in semi-arid areas
420 across the globe 1981–2007 — an Earth Observing Satellite based analysis of trends and drivers.
421 *Remote Sen. Environ.* 121: 144-158.

422

423 Fisher, J., Tu, K. P., and Baldocchi, D. D. 2008. Global estimates of the land-atmosphere water
424 flux based on monthly AVHRR and ISLSCP-II data, validated at 16 FLUXNET sites, *Remote*
425 *Sens. Environ.*, 112: 901–919.

426

427 Garratt J.R., Hicks B.B. 1973. Momentum, heat and water vapor transfer to and from natural and
428 artificial surfaces. *Quart. J. Roy. Meteorol. Soc.* 99:680–687.

429

430 Guzinski, R., Anderson, M.C., Kustas, W.P., Nieto, H., Sandholt, I. 2013. Using a thermal-based
431 two source energy balance model with time-differencing to estimate surface energy fluxes with
day-night MODIS observations. *Hydrol. Earth Syst. Sci.* 17: 2809–2825.

- 432 Humes, K. S., Kustas, W.P, Moran, M. S., Nichols W. D., Weltz, M. A. 1994. Variability in
433 emissivity and surface temperature over a sparsely vegetated surface. *Water Resour. Res.* 30(5):
434 1299-1310.
- 435 Kondo, J., Ishida, S., 1997. Sensible heat flux from the Earth's surface under natural convective
436 conditions. *J. Atmos. Sci.* 54 (4), 498–509.
- 437 Kustas, W.P. 1990. Estimates of evapotranspiration with a one- and two-layer model of heat
438 transfer over partial canopy cover. *J. Appl. Meteorol.* 29(8):704-715.
- 439 Kustas, W.P., Norman, J.M., 1999. Evaluation of soil and vegetation heat flux pre-dictions using
440 a simple two-source model with radiometric temperatures for partial canopy cover. *Agric. For.*
441 *Meteorol.* 94 (1), 13–29.
- 442 Kustas, W.P., Norman, J.M. , Schugge, T.J., Anderson, M.C. 2004. Mapping surface energy
443 fluxes with radiometric temperature. In Quattrochi, D. and Luvall, J. (eds.) *Thermal Remote*
444 *Sensing in Land Surface Processes*, CRC Press Boca Raton, FL. 440 pp.
- 445 Kustas, W.P., Anderson, M.C., Norman, J.M. and Li, F. 2007. Utility of radiometric
446 aerodynamic temperature relations for heat flux estimation. *Bound.-Layer Meteorol.* 122:167-
447 187.
- 448 Kustas, W.P., Anderson, M.C., 2009. Advances in thermal infrared remote sensing for land
449 surface modeling. *Agric. For. Meteorol.*,149: 2071–2081.
- 450 Lhomme, J.P., Chehbouni, A., Monteny, B. 2000. Sensible heat flux-radiometric surface
451 temperature relationship over sparse vegetation: Parameterizing B-1. *Bound.-Layer Meteor.*,
452 97(3): 431-457.
- 453 Lhomme, J.-P., Troufleau, D., Monteny, B., Chehbouni, A., Baudmin, S. 1997. Sensible heat
454 flux and radiometric temperature over a sparse Sahelian vegetation II. A model for the kB^{-1}
455 parameter. *J. Hydrol.* 188-189:839-854.
- 456 Matsushima, D. 2005. Relations between aerodynamic parameters of heat transfer and thermal-
457 infrared thermometry in the bulk surface formulation. *J. Meteorol. Soc. Japan*, 83(3): 373-389.
- 458 McNaughton, K.G., van den Hurk, B.J.J.M. 1995. A 'Lagrangian' revision of the resistors in the
459 two-layer model for calculating the energy budget of a plant canopy. *Bound.-Layer Meteorol.*
460 74: 261-288
- 461 Merlin O., Chebhouni, A. 2004. Different approaches in estimating heat flux using dual angle
462 observations of radiative surface temperature, *Inter. J. Remote Sens.* 25: 275-289.

463 Morillas, L., García, M., Nieto, H., Villagarcía, L., Sandholt, I., Gonzalez-Dugo, M.P. Zarco-
464 Tejada, P.J., Domingo, F. 2013. Using radiometric surface temperature for energy flux
465 estimation in Mediterranean drylands from a two-source perspective. *Remote Sens. Environ.*
466 136, 234–246.

467 Norman J.M., Kustas W.P., Humes, K.S. 1995. A two-source approach for estimating soil and
468 vegetation energy fluxes from observations of directional radiometric surface temperature. *Agric.*
469 *For. Meteorol.* 77:263–293.

470 Owen, P.R., and Thompson, W.R. 1963. Heat transfer across rough surfaces. *J. Fluid. Mech.*
471 15:321-334.

472 Ryu, Y., Baldocchi, D.D., Ma, S., and Hehn, T. 2008. Interannual variability of
473 evapotranspiration and energy exchange over an annual grassland in California. *J. Geophys. Res.*
474 113 D09104, doi:10.1029/2007JD009263.

475 Sauer, T.J., Norman, J.M., Tannar, C.B., and Wilson, T.B. 1995. Measurement of heat and
476 vapor transfer coefficients at the soil surface beneath a maize canopy using source plates. *Agric.*
477 *For. Meteorol.* 75:161-189.

478 Stewart, J.B. 1995. Turbulent surface fluxes derived from radiometric surface temperature of a
479 sparse prairie grass. *J. Geophys. Res.* 100(D12):25,429-25,433.

480 Stewart, J.B., Kustas, W.P., Humes, K.S., Nichols, W.D., Moran, M.S. and de Bruin, H.A.R.
481 1994. Sensible heat flux-radiometric surface temperature relationship for 8 semi-arid areas. *J.*
482 *Appl. Meteorol.* 33:1110-1117.

483 Su Z, Schmugge T, Kustas WP, Massman WJ. 2001. An evaluation of two models for estimation
484 of the roughness height for heat transfer between the land surface and the atmosphere. *J Appl*
485 *Meteorol* 40:1933–1951.

486

487 Thom, A. S. 1972. Momentum, mass and heat exchange of vegetation. *Q. J. R. Meteorol. Soc.*,
488 98: 124-134.

489

490 Troufleau D, Lhomme J.P., Monteny B., Vidal A. 1997. Sensible heat flux and radiometric
491 surface temperature over sparse Sahelian vegetation. I. An experimental analysis of the kB^{-1}
492 parameter. *J Hydrol* 188–189:815–838

493 Verhoef, A., Allen, S.J., DeBruin, H.A.R., Jacobs, C.M.J., and Heusinkveld, B.G. 1996. Fluxes
494 of carbon dioxide and water vapour from a Sahelian savanna. *Agric. For. Meteorol.* 80: 231-248.

- 495 Verhoef A., De Bruin H.A.R., van den Hurk B.J.J.M. 1997. Some practical notes on the
 496 parameter kB^{-1} for sparse vegetation. J. Appl. Meteorol. 36:560–572
- 497 Verma, S.B. 1989. Aerodynamic resistances to transfers of heat, mass and momentum. IAHS
 498 Pub. No. 177 pp. 13-20.
- 499 Villagarcía, L., Were, A. Domingo, F. García, M. Alados-Arboledas, L. 2007. Estimation of soil
 500 boundary-layer resistance in sparse semiarid stands for evapotranspiration modelling, J. Hydrol.,
 501 342(1–2), 173–183, doi:10.1016/j.jhydrol.2007.05.023.
- 502
 503 Were, A., Villagarcia, L., Domingo, F., Alados-Arboledas, L., and Puigdefabregas, J. 2007.
 504 Analysis of effective resistance calculation methods and their effect on modelling
 505 evapotranspiration in two different patches of vegetation in semi-arid SE Spain. Hydrol. Earth
 506 Sys. Sci. 11: 1529-1542.
- 507
 508 Yang, K., Koike, T., Ishikawa, H., Kim, J., Li, X., Liu, H.Z., Liu, S.M., Ma, Y.M., Wang, J.M.
 509 2008. Turbulent flux transfer over bare-soil surfaces: Characteristics and parameterization. J.
 510 Appl. Meteorol. Climatol., 47(1): 276-290.

511
 512
 513
 514 List of Figure Captions
 515

516 Figure 1. Schematic diagram of one-source and two-source thermal-based models of sensible
 517 heat flux. See text for definition of the symbols used in the one-source model formulations. For
 518 the two-source model (TSEB), T_{SOIL} is the soil surface temperature with associated soil surface
 519 aerodynamic resistance (R_S) and heat flux from the soil (H_S) and T_{CANOPY} is the vegetation
 520 canopy temperature with associated aerodynamic canopy resistance (R_X) and heat flux from the
 521 canopy (H_C). T_{SOIL} and T_{CANOPY} are derived from T_{COMP} and an estimate of fraction vegetation
 522 cover with an initial assumption of canopy transpiration and T_{AC} is the temperature in the
 523 canopy air space which is related to the surface aerodynamic temperature via the surface layer
 524 aerodynamic resistance (R_{AERO}) For details of the TSEB formulations see Norman et al. (1995).
 525

526 Figure 2. Histogram (grey bars) of kB^{-1} values computed for the Balsa Blanca site using $R_{AERO} =$
 527 R_A . Also plotted are the mean (filled circles) and standard deviation (horizontal bars) of the kB^{-1}
 528 values listed in Table 1 staggered in the vertical with the Balsa Blanca identified with the solid
 529 star symbol.

530
 531 Figure 3. The ratio of z_{oh}/z_{om} by inverting the kB^{-1} expression, namely, $z_{oh}/z_{om} = \exp(-kB^{-1})$ for
 532 all the kB^{-1} values listed in Table 1.
 533

534

535

536 Figure 4. The composite radiometric temperature measured by the thermal infrared radiometer,
537 T_{COMP} versus the surface aerodynamic temperature T_{AEROH} computed from Eq. (5) using
538 measurements of H , and u^* and estimates of R_{AH} from Eq. (3) with a) $kB^{-1} = 2.2$ derived for the
539 Balsa Blanca site (see Table 1) and b) $kB^{-1} = 7$, an average value from the semi-arid sites
540 analyzed by Stewart et al. (1987). Line is 1:1 relationship with T_{COMP} .

541

542 Figure 5. Photos of a) typical rock cover in non-canopy covered soil surface at the Balsa Blanca
543 site and b) photo illustrating the strongly clumped nature of the semiarid Mediterranean
544 tussock grassland in southeast Spain during green-up and c) at senescence in late September.

545

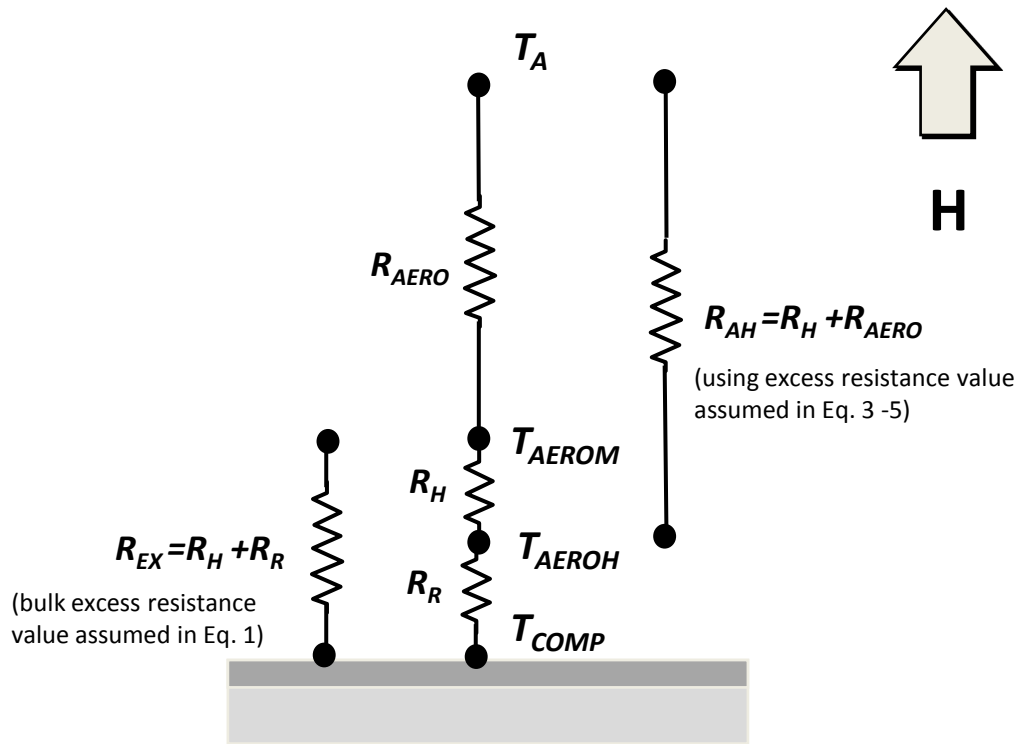
546 Figure 6. Estimated Leaf area index (LAI) and fraction of green LAI (Green LAI) versus Day of
547 Year (DOY) a) from Morillas et al. (2013) using MODIS LAI/fAPAR and a green vegetation
548 fraction, f_G , derived from Fisher et al. (2008); and b) produced using monthly NDVI data from
549 multi-spectral camera and destructive sampling performed at the site between 2009 and 2010.

550

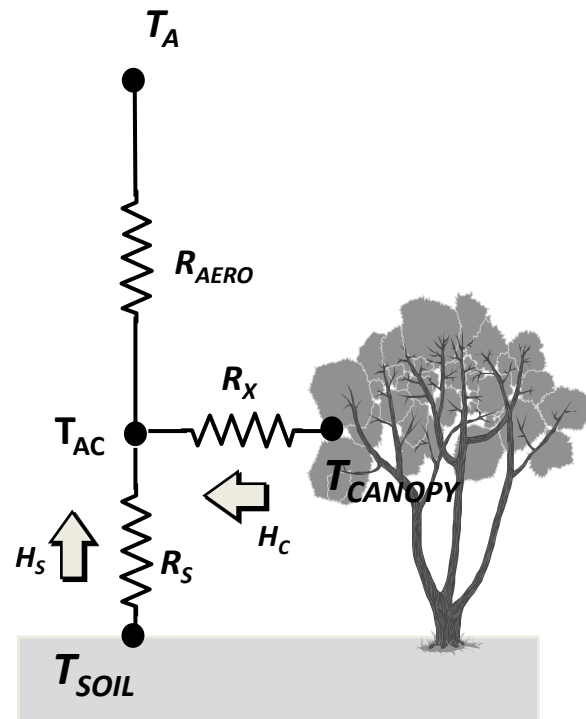
551 Figure 7. Sensitivity in the output from TSEB for a) H and b) LE using original LAI and f_G
552 inputs from Morillas et al (2013) and with the standard soil resistance formulation coefficients c
553 and b ($c=0.0024$, $b=0.012$), with c) H and d) LE computed using modifications to LAI
554 ($LAI \sim 1.75$) and green LAI ($f_G * LAI$) inputs (see Figs. 5 and 6) based on ground observations
555 and with the standard soil resistance formulation coefficients c and b , and with e) H and f) LE
556 computed using modified LAI and green LAI inputs along with assuming a rough soil surface
557 with clumped vegetation which resulted in revising the values of the soil resistance coefficients c
558 and b ($c=0.0038$, $b=0.0605$). See text for more details.

Table 1. Average (avg) and standard deviation (σ) of the kB^{-1} variable based on Eq. (1) and $R_{EX} \sim B^{-1}/u^*$ using the Balsa Blanca site from Morillas et al (2013) and study sites from Stewart et al. (1994), Troufleu et al. (1997) and Verhoef et al. (1997) having vegetation cover (not bare soil). Where available measurements or indirect estimates (*) from the literature of leaf area index (LAI), canopy height (h_c), fractional canopy cover (f_c) are provided from the literature as well as number of data point (n) in the statistics. The symbol NO indicates the authors found no observations or estimates provided.

Project	Surface type	LAI (-)	h_c (m)	f_c (-)	n	KB^{-1} avg	KB^{-1} σ
Balsa Blanca	Tussock grass	1.75	0.7	0.6	4803	2.2	1.7
SEBEX	Fallow Savannah	0.2→0.7 (grass) 0.1→0.6 (shrub)	0.6 (grass) 2.5 (shrub)	0.3* 0.2*	507	5.8	2.9
SEBEX	Open forest	1.3*	4.5	0.3	1142	8.3	3.3
MONSOON 90	Grassland	0.8	0.1	0.35	95	3.8	2.8
MONSOON 90	Shrubland	0.5	0.5	0.26	98	5.6	2.8
Owens Valley	Shrubland	0.48	1	0.25	22	8.0	3.8
Smith Creek Valley	Shrubland	1*	0.75	0.25	69	12.4	5.9
Smoke Creek Desert	Shrubland	NO	0.5*	0.30	79	8.4	4.9
La Crau	Stone/grass	NO	0.1*	0.05	40	4.5	2.1
EFEDA	Vineyard	0.4	1	0.10	246	8.1	2.8
HAPEX-Sahel	Savannah	NO (shrub) NO (grass)	2→2.5 (shrub) 0.5< (grass)	0.2 (shrub) NO (grass)	285	12.4	4.6
HAPEX-Sahel	Fallow Savannah	0.5 (shrub) NO (grass)	3.5 (shrub) 0.2→0.6 (grass)	0.2* (shrub) NO (grass)	1229	8.8	5.6
HAPEX-Sahel	Millet 1992	0.41→2.81	0.76→2.53	0.19→0.56	1011	4	4.4
HAPEX-Sahel	Millet 1991	1.9→2.8	0.72→2.2	0.20→0.30	648	6.7	5.1



a) One-source model



b) Two-source model

